

Prediction of a global climate change on Jupiter

Philip S. Marcus

Department of Mechanical Engineering, University of California, Berkeley, California 94720, USA

Jupiter's atmosphere, as observed in the 1979 Voyager space craft images, is characterized by 12 zonal jet streams and about 80 vortices, the largest of which are the Great Red Spot and three White Ovals that had formed¹ in the 1930s. The Great Red Spot has been observed² continuously since 1665 and, given the dynamical similarities between the Great Red Spot and the White Ovals, the disappearance^{3,4} of two White Ovals in 1997–2000 was unexpected. Their longevity and sudden demise has been explained⁵ however, by the trapping of anticyclonic vortices in the troughs of Rossby waves, forcing them to merge. Here I propose that the disappearance of the White Ovals was not an isolated event, but part of a recurring climate cycle which will cause most of Jupiter's vortices to disappear within the next decade. In my numerical simulations, the loss of the vortices results in a global temperature change of about 10 K, which destabilizes the atmosphere and thereby leads to the formation of new vortices. After formation, the large vortices are eroded by turbulence over a time of ~60 years—consistent with observations of the White Ovals—until they disappear and the cycle begins again.

Long-lived cyclones are essential to my climate cycle, but many investigators do not believe they exist⁶. I therefore begin by arguing for their existence. The argument^{7,8} against long-lived cyclones is that their tangled, filamentary clouds are inconsistent with streamlines of coherent vortices. However, inferring longevity from cloud morphology is difficult. Moreover, cyclonically rotating clouds are currently visible in the same regions where Voyager observed them in 1979, suggesting that the underlying cyclones are long-lived. Figure 1, which compares observed and numerically simulated clouds, attacks the morphology argument. (The Methods section describes these simulations.) The statistically steady equilibrium has two, staggered, opposite-signed rows of vortices called a Kármán vortex street. All the vortices last indefinitely, so the cyclones are long-lived. Because jovian vortices⁹ are patches of nearly uniform potential vorticity q , a vortex is labelled an 'anticyclone' if its $q > 0$ (Fig. 1b). (I adopt a southern hemisphere reference, so anticyclones rotate anticlockwise, but in both hemispheres the anticyclones spin opposite to the planet's rotation.) In Fig. 1c, the centre of an anticyclone has vorticity ω that is also anticyclonic ($\omega > 0$) but is surrounded by a band of cyclonic ω . 'Cyclones' have the opposite arrangement. Although the velocities of cyclones and anticyclones in Fig. 1 are mirror images, their simulated clouds are different because clouds act as particle tracers and in turbulent flows particle paths are not coincident with streamlines. My simulations create clouds where $\omega > 0$ and melt them where $\omega < 0$. Ice-forming and -melting locations differ for cyclones and anticyclones. Figure 1 shows that observed and simulated clouds are similar, that clouds of cyclones and anticyclones are dissimilar, and (most importantly) that twisted, filamentary clouds are consistent with long-lived cyclones.

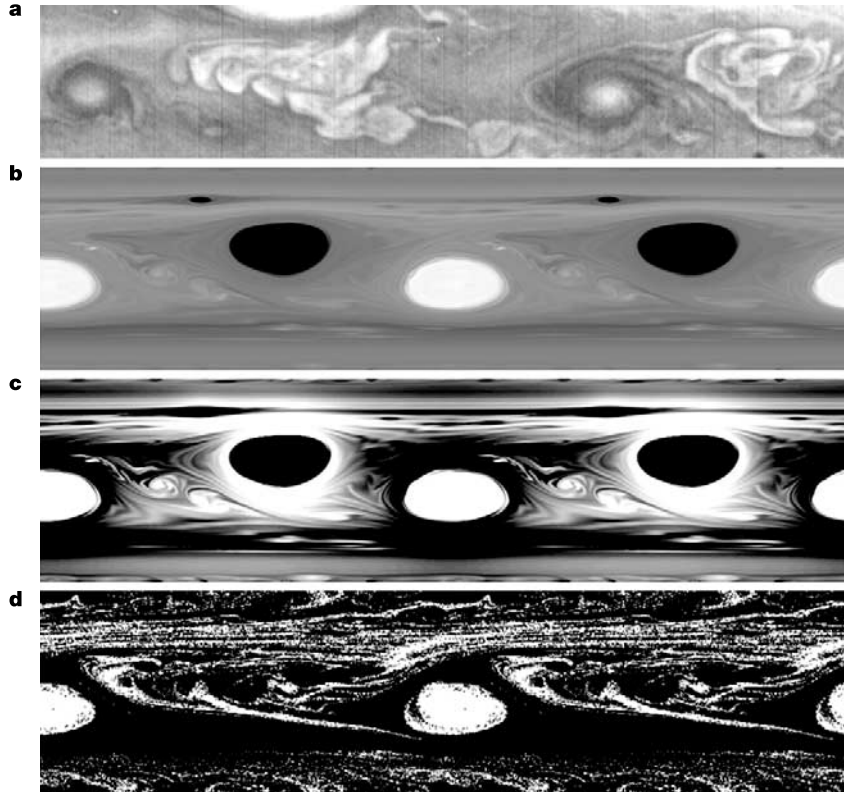


Figure 1 Observed and simulated jovian clouds. **a**, Voyager mosaic showing 2 of the 12 cyclone/anticyclone pairs at 41° S. The clouds of 'cyclones' are large, tangled and filamentary, whereas those of 'anticyclones' are bright, 2:1 ovals surrounded by dark rings. **b**, Simulated potential vorticity q , with cyclonic q shown black and anticyclonic q white. **c**, ω of the same flow in **b** with cyclonic ($\omega < 0$) shown black and anticyclonic ω white. **d**, Simulated clouds of the flow in **b**, where white pixels represent NH_3 ice. For

anticyclones: ice is created in the vortex interior where $\omega > 0$ and there is weak upwelling; ice is rapidly melted in the ring around the vortex where $\omega < 0$; the clouds are ovals (coincident with regions where $\omega > 0$) surrounded by dark rings (coincident with regions where $\omega < 0$). For cyclones: turbulence spreads and twists the clouds created at the peripheral rings (where $\omega > 0$); the turbulence fills the interiors (where $\omega < 0$) with cloud filaments before they melt.

My climate cycle has five stages, the longest of which is the ‘Kármán vortex streets’ stage. I believe that in the current cycle, this stage began in about 1940 and is now ending. With the exception of the Great Red Spot (GRS), all long-lived jovian vortices occur in opposite-signed pairs in streets. Anticyclones are longitudinally staggered with cyclones, so that like-signed vortices are never adjacent (Figs 1 and 2). A westward-going jet stream separates the street’s two rows. The vortices drift and oscillate in longitude with velocities $\sim 3 \text{ m s}^{-1}$ (jet streams and vortex winds are $\sim 100 \text{ m s}^{-1}$). My calculations⁹ showed that an initial row of anticyclones, with no neighbouring cyclones, was unstable: the vortices approached each other, and they all merged. The only way I could maintain them in a row was by arranging them in a vortex street. I found¹⁰ that cyclones and anticyclones repel in this configuration. If, for any reason, two same-signed vortices become adjacent, they rapidly merge. To push an anticyclone past a neighbouring cyclone and make two anticyclones longitudinally adjacent (that is, with no intervening cyclone) requires a perturbation velocity V_{crit} exceeding $\sim 30 \text{ m s}^{-1}$. A new analysis in the Methods section agrees with this finding.

As vortex streets are essential to the climate cycle proposed here, the GRS’s existence outside a street (that is, its uniqueness at its latitude) needs clarification. Jovian vortices are robust because strong Coriolis forces make the atmospheric flow nearly two-dimensional, an environment where vortices thrive. (Three-dimensional flow destroys vortices.) The GRS cannot be part of a street because the street’s cyclones would need to be north of the westward jet stream at 20° S , and no cyclones (not even transients) lie between 20° S and the equator. Their absence is consistent with the flow’s more three-dimensional appearance there (presumably due to the weak Coriolis force). Ephemeral anticyclones often appear at the same latitude as the GRS but, because there are no nearby cyclones to repel them, they merge with it, leaving the GRS as the only long-lived vortex there.

As $V_{\text{crit}} \approx 30 \text{ m s}^{-1}$ is needed to disrupt a vortex street and the available perturbations from turbulence and longitudinal oscillations are only $\sim 3 \text{ m s}^{-1}$, it was surprising in 1994 when two White Ovals became closely spaced, drifted together for 3 years and then merged. These events marked the cycle’s ‘Trapping and vortex merging’ stage. Experiments¹¹ and calculations¹² show that the trough of a Rossby wave (on an eastward jet stream) can trap vortices, making them and the trough drift together⁵ (Fig. 3). Vortices are trapped because anticyclones are repelled by the cyclonic outside edge of the trough as if it were a cyclone.

Varying the size or area A_C of the trapped cyclone while holding all other parameters to be those of the White Ovals, we found⁵ three critical areas: $A_C^{\text{escape}} > A_C^{\text{trap}} > A_C^{\text{merge}}$. Untrapped vortices get trapped when $A_C < A_C^{\text{trap}}$; when $A_C > A_C^{\text{escape}}$, initially trapped

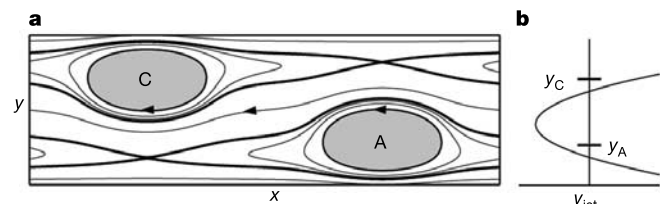


Figure 2 Dynamics of two vortices in a Kármán street. **a**, Streamlines of one period (in the east–west or x direction) of an infinitely long vortex street with cyclone C and anticyclone A. Jovian anticyclones (cyclones) are on the poleward (equatorial) side of the westward jet. There are three pairs of opposite-signed vortices straddling the jet at 34° S (in which the anticyclones are the White Ovals), 12 at 41° S , and so on. The outermost closed streamlines (OCS) which connect the stagnation points (where streamlines cross) are heavy lines. Outside the OCS the streamlines are open. To represent the White Ovals, I would need to increase the spacings between the vortices by a factor of ~ 6 while holding the sizes of the vortices fixed. **b**, The velocity of the jet stream as a function of y . For the numerical experiment described in the Methods section, the initial locations of the latitudes of the centres of the anticyclone and cyclone are y_A and y_C .

vortices escape the trough; and when $A_C < A_C^{\text{merge}}$, the repulsion is so weak that the two trapped anticyclones become adjacent and merge. When $A_C^{\text{trap}} > A_C > A_C^{\text{merge}}$, the trough ‘squeezes’ trapped vortices together⁵, causing V_{crit} to decrease from $\sim 30 \text{ m s}^{-1}$ to $\sim 3 \text{ m s}^{-1}$. We believe that two White Ovals (and a cyclone) drifted together (that is, were trapped) in 1994–97 because A_C became less than A_C^{trap} . Just before their merger, they collided with an untrapped cyclone (Fig. 3). This created a perturbation greater than $V_{\text{crit}} \approx 3 \text{ m s}^{-1}$, and the Ovals merged. We showed⁵ that if A_C continues to decay, vortices in a street become trapped and merge until only one vortex pair survives.

The Methods section shows that vortex mergers lead to ‘Global temperature changes’, the cycle’s next stage, in which the temperature T near the equator (poles) rises (falls) by $\sim 10 \text{ K}$. Currently the weather layer (containing the clouds and vortices) is nearly isothermal in latitude. This is surprising and not understood. A balance between cooling via blackbody radiation and heating from the Sun (a function of latitude) and internal sources would make the poles $\sim 30 \text{ K}$ cooler than the equator¹³. Most solar heat is absorbed in, or just below, the weather layer, so deep convection cannot make its T uniform¹⁴. Consistent with theory¹⁵ my calculations show that when there are several vortices per westward jet, the velocity \mathbf{v} is chaotic and chaotic mixing of T makes the layer isothermal. An exception is that the T within and exterior to the vortices do not mix. The strong gradient of q circumscribing each vortex acts as a barrier to transport¹⁶. Chaotic mixing explains not only why the layer is isothermal but also why cyclones (anticyclones) remain warm (cool). My calculated T is insensitive to details of \mathbf{v} as long as \mathbf{v} is chaotic and $D/|\mathbf{v}| \ll \tau_{\text{rad}}$, that is, the advective time (a few days) is much less than the radiative time ($\tau_{\text{rad}} \approx 7$ years), where D is a vortex diameter. After the vortices in the streets merge, the chaos and mixing diminish, T relaxes toward its radiative equilibrium, a large latitudinal gradient in T forms, and at subtropical latitudes the T at the layer’s bottom (where the solar heat is absorbed) increases by $\delta T \approx 6 \text{ K}$. (Note that vortices create high

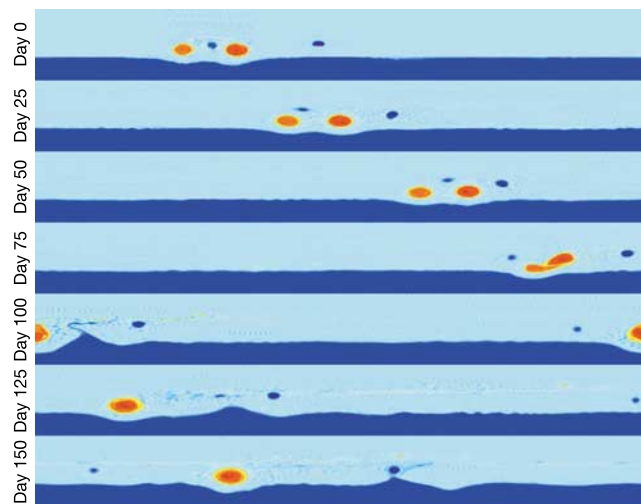


Figure 3 Frames of q from a simulation movie. (Available as Supplementary Information.) The domain is periodic in x . Initially, two anticyclones (red) and one cyclone (blue) are trapped in the trough of a Rossby wave (interface between light and dark blue), and there is also a small cyclone 25,000 km east of the trough. The initial conditions mimic the White Ovals before their merger⁵. For the first 60 days, the trapped vortices drift eastward at $\sim 1 \text{ m s}^{-1}$ and are closely spaced inside the trough. The centre cyclone oscillates between the outer anticyclones. (Without the trough, they spread apart at speeds of $\sim 5 \text{ m s}^{-1}$.) The untrapped cyclone initially moves west, but after day ~ 60 moves east because it is repelled by the vortices in the trough. The repulsion perturbs the central cyclone, allowing it to pass to the west of the anticyclone on its westward side at day ~ 60 . The anticyclones are then adjacent and merge (days 75–100). The remaining cyclones merge ~ 1 year later.

clouds that absorb and reflect heat, and thereby cool the bottom of the weather layer. Thus the loss of vortices increases δT for a second, independent reason.) Currently the weather layer is not strongly stratified. The Methods section shows that a ~ 6 K warming is not enough to destabilize the layer to convection, but is strong enough to decrease the Rossby deformation radius L_r by 30% which will ‘Destabilize jet streams and form new vortices’. This is the cycle’s next stage. Calculations show that after the vortices merge, leaving only one pair per westward jet stream, the flow is stable if L_r is held fixed. However, when L_r is reduced in the calculations to be in accord with temperature changes, within a few months waves form on the jet streams. They grow, break and roll-up into new vortices, in agreement with others’ calculations¹⁷ of baroclinic jet instabilities. I believe that the break-up of the band of clouds in 1938–39 that formed the White Ovals is an example of this instability. A necessary condition for linear instability¹⁸ of a steady jet is that its $q(y)$ has extrema. Extrema are created when L_r decreases: equation (1) in Methods shows that if L_r^2 decreases by half while \mathbf{v} remains fixed, then q changes from $q_{\text{jet}}^{\text{old}}$ to $q_{\text{jet}}^{\text{new}}(y) \equiv q_{\text{jet}}^{\text{old}}(y) - \psi_{\text{jet}}(y)/[L_r^{\text{old}}]^2$, which generally has large extrema because the velocity of the jet stream $v_{\text{jet}}(y)$ (and therefore the stream function of the jet stream $\psi_{\text{jet}}(y)$) is oscillatory.

New vortices rapidly shrink until they look like the vortex streets in the cycle’s first stage. The newly formed White Ovals shrank¹ quickly from $\sim 90,000$ km to $\sim 20,000$ km. From 1950 to 2000, they slowly shrank to $\sim 10,000$ km. Calculations show that the ‘Slow erosion of vortex streets’ stage continues for ~ 60 years. This is the cycle’s final stage. Figure 2 explains the shrinkage. Closed streamlines surround vortices. The outermost closed streamline (OCS) contains stagnation points. When a vortex forms that is larger than its OCS, the q outside the OCS quickly pulls away until the vortex lies within its OCS. This was the likely cause of the Ovals’ initial rapid shrinkage. A vortex random-walks around its equilibrium at the centre of its OCS owing to turbulence. When its edge bumps the OCS, its outer q is carried to a stagnation point where it is stripped away. The stronger the turbulence, the smaller the surviving vortex¹⁹. Turbulent erosion is analogous to carrying a full cup of coffee: with steady (laminar) hands, the cup remains filled to its brim (OCS). With unsteady hands, the mean surface of the coffee is below the brim. The distance from the brim to the surface increases with increasing unsteadiness, so the volume of coffee (vortex area) decreases with increasing unsteadiness (turbulence). Turbulent erosion is more complex for vortex streets because the OCSs are highly elongated, but it explains observations that show that the Ovals’ slow shrinkages between 1950 and 2000 were temporally correlated with their reversals in direction¹. Before 1994, the Ovals and cyclones made long oscillations in longitude with periods of ~ 15 years. Their erosion had nearly stopped because they were inside and generally far from their OCSs. However, every half-period, an Oval and cyclone approached each other (and a stagnation point on the OCS) and reversed directions. I argue that during each encounter they eroded. Calculations show that ~ 4 periods (~ 60 years for the Ovals) are needed for A_C to become less than A_C^{trap} . Turbulent erosion is the slowest part of the cycle, and sets its period of $(60 + \tau_{\text{rad}}) \approx 70$ years.

I predict an imminent, dramatic change in the jovian climate as part of a ~ 70 -year cycle. Calculations show that cyclones are required to maintain rows of anticyclones. The cyclones’ decay inevitably destroys anticyclones. I believe that the disappearance of two White Ovals at 34° S in the late 1990s was due to the decay of cyclones, and that it was part of a recurring cycle—the disappearance and re-appearance¹ of anticyclones at 34° S in the 1930s was part of the previous cycle. For a cycle to exist, feedback is needed between the disappearance of anticyclones and the dynamics that regenerates them. An obvious feedback is heat transport. Calculations show that chaotic mixing of heat owing to the chaos produced by multiple vortex pairs in a street makes the weather layer isothermal. Destruction of the vortices reduces the chaos and decreases the

mixing. The jovian jet streams are easily destabilized by small temperature changes. Generically, jet streams go unstable via growing waves that break, roll up and create rows of vortices^{10,17,18,20,21}. Therefore, I expect vortices to re-emerge from destabilized jet streams. The true tests of predictions are observations, and there are many to look for within the next decade: the bunching together of vortices (especially at 41° S) followed by their merging, cooling of the poles and warming of the equator, and instabilities of the jet streams indicated by the break-up of circumferential bands of clouds into new ‘spots’. □

Methods

Calculations use the quasigeostrophic²² (QG) equation for the potential vorticity q :

$$q \equiv \nabla^2 \psi - \psi/L_r^2 + \beta y; \quad dq/dt \equiv (\partial/\partial t + \mathbf{v} \cdot \nabla)q = 0 \tag{1}$$

with stream function ψ , velocity $\mathbf{v} \equiv \hat{\mathbf{z}} \times \nabla \psi$, vertical unit vector $\hat{\mathbf{z}}$, Coriolis parameter β , north–south coordinate y and Rossby deformation radius L_r . In Fig. 1, the initial distributions of cyclonic and anticyclonic q are mirror images, and owing to the symmetry of equation (1) remain so. I decompose \mathbf{v} into a jet stream component $v_{\text{jet}}(y)\hat{\mathbf{x}}$ plus a remainder consisting of vortices and turbulence $\mathbf{v}'(x, y, t)$, and define the vorticity $\omega \equiv \hat{\mathbf{z}} \cdot (\nabla \times \mathbf{v}')$. In the upper weather layer, anticyclonic (cyclonic) ω creates upward (downward) flow¹⁰. In a subadiabatic atmosphere, upwelling cools the fluid, so I simulate the formation of NH_3 ice clouds by adding white pixels (that advect with \mathbf{v}) at a rate proportional to the local anticyclonic ω (and upwelling). I melt ice (that is, destroy white pixels) in regions with cyclonic ω . The vortex centres have weak $|\omega|$ and are surrounded by small-area rings (with widths $\sim L_r$) with opposite-signed ω (Fig. 1). The rings’ $|\omega|$ are large; the circulation of each vortex $\int \omega \, dA$ is zero—as it must be for a compact QG vortex. The advective timescale of turbulent transport is between the slow timescale of melting/creation in the small- $|\omega|$ interior and the fast timescale of the melting/creation in the large- $|\omega|$ ring. For an anticyclone: ice is created and well-mixed in the vortex interior before it advects out, so the interior is uniformly bright. When advected out of the centre, the ice melts quickly leaving the surrounding ring ice-free and dark. For a cyclone: ice is rapidly created in the ring and advects to its surroundings. It remains a long time in the interior where it is stretched into filaments because the interior’s melting time is long.

Figure 2 shows why opposite-signed vortices in a Kármán vortex street straddling a westward jet stream repel. Vortices advect with the ambient \mathbf{v} . The velocity due to a QG vortex falls off exponentially¹⁰ at distances greater than L_r , so for widely separated vortices, $v_{\text{jet}}(y)$ dominates. Let a cyclone approach an anticyclone from the west. Initially, they advect with velocities $v_{\text{jet}}(y_C)$ and $v_{\text{jet}}(y_A)$, where y_C and y_A are the latitudes of the centres of the cyclone and anticyclone. Figure 2 is in the reference frame with $v_{\text{jet}}(y_C) + v_{\text{jet}}(y_A) = 0$, so initially $v_{\text{jet}}(y_C) > 0$ and $v_{\text{jet}}(y_A) < 0$, and the vortices approach each other. When the vortex separation becomes less than L_r , the anticyclone (cyclone) causes the cyclone (anticyclone) to orbit anticlockwise (clockwise) around it. This pushes both vortices south. The shear of the westward jet stream, $\sigma(y) \equiv -dv_{\text{jet}}/dy$, is negative (positive) on its northern (southern) side, so as the vortices move south, $v_{\text{jet}}(y_C)$ becomes more negative and $v_{\text{jet}}(y_A)$ more positive. The vortices repel. We showed numerically² that a cyclone and anticyclone would need to approach initially at velocities greater than a critical value $V_{\text{crit}} \approx 30 \text{ m s}^{-1}$ to not be completely repelled and to pass by each other (resulting in adjacent like-signed vortices). I can obtain this same value of V_{crit} analytically. An anticyclone’s east–west velocity v_A is primarily due to v_{jet} , so a change in its latitude Δy_A changes v_A by:

$$\Delta v_A \approx \Delta y_A (dv_{\text{jet}}/dy) = -\sigma(y_A) \Delta y_A \tag{2}$$

the anticyclone’s Δy_A in Fig. 2 is due to the cyclone’s velocity, which, using the Biot-Savart law (assuming the vortex separation is $\sim L_r$), has strength $A_C q_C / 2\pi L$ where L is the distance between the vortices and A_C and q_C are the area and q of the cyclone. Therefore, $|\Delta y_A| \approx A_C q_C \Delta t / 2\pi L$, where Δt is the duration of the vortex/vortex encounter. Thus

$$|\Delta v_A| = |\sigma(y_A) A_C q_C \Delta t / 2\pi L| = |\sigma(y_A) A_C q_C / 2\pi v_A| \tag{3}$$

where I used $L/\Delta t \approx |v_A|$. In order for the vortices to repel, $|v_A| < |\Delta v_A|$, or using equation (3):

$$|v_A| < \sqrt{\sigma(y_A) A_C q_C / 2\pi} \equiv V_{\text{crit}} \tag{4}$$

Thus, $V_{\text{crit}} \equiv \sqrt{\sigma(y_A) A_C q_C / 2\pi} = 26 \text{ m s}^{-1}$, where we used parameter values of the White Ovals⁵.

To find changes in the jovian T , I solved numerically the advection equation²³ for T in a thin weather layer differentially heated by the Sun, uniformly heated from below and radiatively cooled. (I used an albedo that gives an average (over the entire atmosphere) incident solar flux of 8.4 W m^{-2} , and I used an internal flux of 5.7 W m^{-2} .) The advection velocity \mathbf{v} is computed from equation (1) and changes with the cycle’s stages. The radiative time $\tau_{\text{rad}} \equiv c_v \rho H / 4aT^3 \approx 7$ years, with heat capacity c_v , density ρ , layer thickness $H = 10$ km, and Stefan’s constant a . The layer is not strongly stratified; the temperature difference δT between its bottom and top is not much smaller than the value of a neutrally stratified layer $\delta T|_s \equiv gH/c_p = 47$ K, where g is the acceleration due to gravity. Although the jovian δT cannot be measured directly, $L_r(\theta) \equiv \sqrt{gH(\delta T|_s - \delta T)/T/2\Omega \sin\theta}$ is well known¹⁰, where $2\pi/\Omega$ is the jovian period and θ the latitude. This expression gives $\delta T = 35$ K. Heating the bottom of the weather layer by more than $(\delta T|_s - \delta T) = 12$ K would destabilize it to convection; heating it by only ~ 6 K decreases $L_r(\theta)^2$ by half.

Received 21 January; accepted 9 March 2004; doi:10.1038/nature02470.

1. Rogers, J. H. *The Giant Planet Jupiter* (Cambridge Univ. Press, Cambridge, 1995).
2. Hook, R. A spot in one of the belts of Jupiter. *Phil. Trans.* **1**, 3 (1665).

3. Sánchez-Lavega, A. *et al.* Interactions of Jovian White Ovals BC and DE in 1998 from Earth-based observations in the visual range. *Icarus* **142**, 116–124 (1999).
4. Sánchez-Lavega, A. *et al.* The merger of two giant anticyclones in the atmosphere of Jupiter. *Icarus* **149**, 491–495 (2001).
5. Youssef, A. & Marcus, P. S. The dynamics of jovian white ovals from formation to merger. *Icarus* **162**, 74–93 (2003).
6. MacLow, M.-M. & Ingersoll, A. P. Merging of vortices in the atmosphere of Jupiter: an analysis of Voyager images. *Icarus* **65**, 353–369 (1986).
7. Neelin, M. Rossby solitary vortices, on giant planets and in the laboratory. *Chaos* **4**, 187–202 (1994).
8. Sutyrin, G. Long lived planetary vortices and their evolution: Conservative intermediate geostrophic model. *Chaos* **4**, 203–212 (1994).
9. Marcus, P. S. Numerical simulations of Jupiter's Great Red Spot. *Nature* **331**, 693–696 (1988).
10. Marcus, P. S. Jupiter's Great Red Spot and other vortices. *Annu. Rev. Astron. Astrophys.* **31**, 523–573 (1993).
11. Solomon, T. H., Holloway, W. J. & Swinney, H. L. Shear flow instabilities and Rossby waves in barotropic flow in a rotating annulus. *Phys. Fluids* **5**, 1971–1982 (1993).
12. Marcus, P. S. & Lee, C. A model for eastward and westward jets in laboratory experiments and planetary atmospheres. *Phys. Fluids* **10**, 1474–1489 (1998).
13. Flasar, F. M. Global dynamics and thermal structure of Jupiter's atmosphere. *Icarus* **65**, 280–303 (1986).
14. Gierasch, P. J. Radiative-convective latitudinal gradients for Jupiter and Saturn models with a radiative zone. *Icarus* **142**, 148–154 (1999).
15. Ottino, J. M. *The Kinematics of Mixing: Stretching, Chaos, and Transport* (Cambridge Univ. Press, Cambridge, 1989).
16. Solomon, T. H., Weeks, E. R. & Swinney, H. L. Chaotic advection in a two-dimensional flow: Levy flights and anomalous diffusion. *Physica D* **76**, 70–84 (1994).
17. Panetta, R. L. Zonal jets in wide baroclinically unstable regions: Persistence and scale selection. *J. Atmos. Sci.* **50**, 2073–2106 (1993).
18. Drazin, P. G. & Reid, W. *Hydrodynamic Stability* (Cambridge Univ. Press, Cambridge, 1981).
19. Humphreys, T. D. *Jovian Kármán Vortex Streets as Attractors in Turbulent Zonal Flow*. Thesis, Univ. California, Berkeley (2000).
20. Dowling, T. E. & Ingersoll, A. P. Jupiter's Great Red Spot as a shallow water system. *J. Atmos. Sci.* **46**, 3256–3278 (1989).
21. Marcus, P. S. Vortex dynamics in a shearing zonal flow. *J. Fluid. Mech.* **215**, 393–430 (1990).
22. Pedlosky, J. *Geophysical Fluid Dynamics* (Springer, New York, 1987).
23. Chandrasekhar, S. *Hydrodynamic and Hydromagnetic Stability* (Oxford Univ. Press, Oxford, 1961).

Supplementary Information accompanies the paper on www.nature.com/nature.

Acknowledgements The author thanks T. Kundu for cloud simulations and X. Asay-Davis, S. Shetty and C.-H. Jiang for calculations of temperature changes. The work was supported by the NASA Origins Program, the NSF Astronomy and Plasma Physics Programs and LANL. Computing resources were supplied by NPACI (supported by the NSF).

Competing interests statement The author declares that he has no competing financial interests.

Correspondence and requests for materials should be addressed to the author (pmarcus@me.berkeley.edu).

The ultimate speed of magnetic switching in granular recording media

I. Tudosa¹, C. Stamm¹, A. B. Kashuba², F. King³, H. G. Siegmann¹, J. Stöhr¹, G. Ju⁴, B. Lu⁴ & D. Weller⁴

¹Stanford Synchrotron Radiation Laboratory, PO Box 20450, Stanford, California 94309, USA

²Landau Institute for Theoretical Physics, Kosygin str. 2, Moscow 117940, Russia

³Stanford Linear Accelerator Center, Stanford University, Stanford, California 94309, USA

⁴Seagate Technology LLC, Pittsburgh, Pennsylvania 15222, USA

In magnetic memory devices, logical bits are recorded by selectively setting the magnetization vector of individual magnetic domains either 'up' or 'down'. In such devices, the fastest and most efficient recording method involves precessional switching^{1–4}: when a magnetic field B_p is applied as a write pulse over a period τ , the magnetization vector precesses about the field until $B_p\tau$ reaches the threshold value at which switching occurs. Increasing the amplitude of the write pulse B_p might therefore substantially shorten the required switching time τ and allow for

faster magnetic recording. Here we use very short pulses of a very high magnetic field⁵ to show that under these extreme conditions, precessional switching in magnetic media supporting high bit densities no longer takes place at well-defined field strengths; instead, switching occurs randomly within a wide range of magnetic fields. We attribute this behaviour to a momentary collapse of the ferromagnetic order of the spins under the load of the short and high-field pulse, thus establishing an ultimate limit to the speed of deterministic switching and magnetic recording.

Our conceptually simple technique, which could also be used to study the dynamics of ferromagnetic spins underlying many applications and promising developments in magnetism^{6–8}, utilizes relativistic electron bunches of energy 28 GeV from the Stanford Linear Accelerator to generate unique short and strong magnetic field pulses^{5,9}. Our magnetic field resembles the field generated by a straight current-carrying wire, with the familiar closed circular magnetic field lines about the beam direction with the field strength decreasing as $1/R$ with the distance R from the centre of the beam. The electron beam is focused to a cross-section of $10.8 \times 7.4 \mu\text{m}$ (full-width at half-maximum) in the x - y plane of the sample surface, perpendicular to the z propagation direction, which lies along the surface normal. Along z , the electron distribution is gaussian with a variance of $\sigma_z = 0.7 \text{ mm}$ in the laboratory frame, giving a pulse duration of $\tau = \sigma_z/c = 2.3 \times 10^{-12} \text{ s}$, where c is the speed with which the electrons travel. For all practical purposes that speed is equal to the speed of light.

With the films magnetized perpendicular to the film plane, the magnetic field B_p and magnetization M are orthogonal everywhere. This is the optimum geometry to induce a precessional motion of M about the perpendicular B_p field, which lies in the magnetically hard plane of the film. Once M has precessed about B_p by an angle large enough to cross the hard plane of the sample, it will continue to relax by itself into the opposite direction. Hence in the end it has switched from one easy direction into the opposite easy direction. If however B_p ceases to exist before M has reached the hard plane, M is expected to relax back to its original perpendicular direction, hence no switch is observed. The condition for switching is that the angle of precession $\phi = \omega\tau \geq \pi/2$. As the angular velocity ω is determined by B_p , we obtain the switching condition $B_p\tau \geq \text{const}$.

To test this switching, we prepared 14-nm-thick films of perpendicular granular magnetic recording media of the CoCrPt-type such as recently used in high-density magnetic recording¹⁰. The main condition for high-density recording is that the grains are decoupled so that the medium can sustain narrow transitions between 'up' and 'down' bits. The decoupling of the grains occurs through segregation of Cr to the grain boundaries induced by deposition at elevated temperature. The grain size was determined by X-ray diffraction to be $20 \pm 5 \text{ nm}$. This grain size is so small that the magnetic field B_p is homogeneous over the grain size to better than 0.1% over the R -range of interest. We can then assume that the switching of a grain occurs in a homogeneous applied field. As a substrate, we have used glass with appropriate thin buffer layers, with and without adding a soft magnetic underlayer such as needed in perpendicular recording¹⁰.

The top left panel of Fig. 1 displays contour lines of constant B_p in the film plane. B_p is the peak strength of the gaussian magnetic field pulse calculated from the electron bunch parameters as $B_p = 54.7/R$ where R is measured in micrometres and B_p in tesla. The dark central spot indicates the size of the electron beam focus, close to which no data are obtained owing to beam damage in the sample. The scale is chosen to be the same as in the actual magnetic switching patterns recorded in the other panels of Fig. 1.

Before exposure, the samples were magnetized perpendicular to the film plane into what we shall call the 'up' direction. We recorded patterns on the same sample corresponding to a single shot (pulse),